ESKİŞEHİR TEKNİK ÜNİVERSİTESİ BİLİM VE TEKNOLOJİ DERGİSİ B- TEORİK BİLİMLER

Eskişehir Technical University Journal of Science and Technology B- Theoretical Sciences

2023, 11(2), pp. 125-142, DOI: 10.20290/estubtdb.1282541

RESEARCH ARTICLE

VIBRATIONAL SPECTROSCOPIC STUDY OF PYRIDINE AND PYRIMIDINE LIGANDS COORDINATED WITH ANTIMONY (III) COMPLEXES: INSIGHTS FROM DFT CALCULATIONS

Berna ÇATIKKAŞ*[1], Özge ŞAHİNLER[2]

*[1]Department of Physics, Faculty of Art and Science, Hatay Mustafa Kemal University, Hatay, Türkiye
[2]Department of Physics, Institute of Sciences, Hatay Mustafa Kemal University, Hatay, Türkiye

ABSTRACT

By employing the Scaled Quantum Mechanics Force Field (SQMFF) methodology, a comprehensive analysis was conducted to assign the vibrational spectra of three antimony (III) compounds, [1a-3a], that possess pyridine and pyrimidine ligands. The potential energy distribution (PED) was calculated and utilized to assign the IR spectra of the antimony (III) compounds. The theoretical frontier molecular orbital descriptors, the partial and total density of state distribution (TDOS, PDOS), molecular electronic potential surface map (MEP), nonlinear optical properties (NLO) of these complexes also were computed and investigated. The DFT/B3LYP/GEN (C, H, N, Cl: 6-31G(d,p) and Sb: LanL2DZ) level was utilized for all DFT calculations using the Gaussian 09W program. Furthermore, theoretical frontier molecular orbital descriptors, including electronegativity, chemical potential, softness, electrophilicity index, and electron affinity for six antimony (III) compounds were calculated ([1a/1b-3a/3b]). The results showed that, the ionization potential energy value of the [3a], which had the lowest experimental Leishmania activity, was also found to be the lowest among the others.

Keywords: Antimony (III) compounds, Scaled Quantum Mechanical Force Field, Nonlinear Optics, Infrared Spectra, Density Functional Theory

1. INTRODUCTION

Although antimony is known to be poisonous and carcinogenic, it has been used in medicine for several centuries [1]. The use of antimony complexes ranges from cosmetics to medicine to ancient Egypt [2,3]. The use of antimony in medicine has been widely reported in publications since ancient times [4,5]. Antimony compounds against microbes and parasites are widely used in many applications in medicine [6–9]. Strong antiproliferative activity is shown by antimony(III) complexes against human cancer cells. Some pentavalent antimony compounds are now used effectively in medicine to treat leishmaniasis [10]. Medical practice studies on the use of antimony compounds for anti-leishmania disease have already been published [11–13]. The use of antimony compounds as anthelminthic [10], antitrypanosomal [13,14], antibacterial [15,16], antifungal [17], and anticancer [18–21] agents is just one of the many possible applications for these compounds in the fields of medicine and pharmacy. Additionally, antimony compounds are widely used as catalysts in organic synthesis [14–16].

In 2007, Khalil et al., in their study with antimony complexes of planar tridentate pyridine ligands, showed that 2-acetylpyridine and tridentate Schiff base ligands derived from various acid hydrazides and Sb complexes are soluble in water. It has been concluded that it can be useful in the treatment of various health problems as it is water soluble [17]. Six new $SbBr_3$-Py (Py: Pyridine) crystalline complexes were obtained and structurally characterized in the literature [18]. The structural characteristics of two novel $SbCl_3$-Py crystalline complexes were obtained by Dovydova et al. [19].

*Corresponding Author: berna@mku.edu.tr
Received: 13.04.2023 Published:28.08.2023

To investigate vibrational and electronic properties, Density functional theory (DFT) evaluation of complicated inorganic molecules such as Antimony (III) coordination compounds before experimentation can save valuable resources and time, and increase the probability of obtaining meaningful results. Antimony (III) containing complexes have been found to exhibit greater efficacy in treating when compared to free ligands. Theoretical studies with antimony complexes are very few in the literature. Theoretical DFT-based QSAR research and glutathione reductase inhibitory action of the title complexes were reported by Tunç et al [20–22]. Tunç et al. synthesized and studied several novel antimony(III) complexes, and they looked into the compounds' anti-leishmanial properties [21,22]. In vitro, research was done on the inhibitory effects of promastigote and glutathione reductase. They describe the antibacterial, DNA-cleaving, and glutathione reductase inhibitory activities of fourteen novel antimony(III) complexes [20]. The vibrational harmonic frequencies of the antimony (III) compounds [1a-3a] were calculated in this study using the DFT/B3LYP/GEN (C, H, N, Cl: 6-31G(d,p) and Sb: LanL2DZ) level and the Gaussian 09W program. To acquire a satisfactory assignment for the observed IR spectra of the complexes in the solid phase, the calculated frequency was refined using the Scaled Quantum Mechanical (SQM) approach and Total Energy Distribution (TED). Electronic properties (partial density of states, molecular electrostatic potential and nonlinear optical effect) of the bis($L^{1,2,3}$)trichloroantimony(III) and bis($L^{1,2,3}$)tribromoantimony(III) complexes (*L^1:2-aminopyridine, L^2: 2-amino-5-methylpyridine and L^3: 2-aminopyrimidine* [1a/1b-3a/3b]) have not been done yet. The same level was used to determine the frontier molecular orbital descriptors, total and partial density of state distribution (TDOS, PDOS), molecular electronic potential surface map (MEP), and nonlinear optical properties (NLO) hyper-polarizability effects of six antimony (III) compounds [1a/1b-3a/3b].

2. MATERIALS and METHODS

2.1. Theoretical Calculations

Utilizing the advanced analytical tool Gaussian 09W quantum chemical software [27] and the Lee-Yang-Parr correlation functional (B3LYP) [28–30] approaches with the C, H, N, Cl: 6-31G(d,p) and Sb: LanL2DZ basis set [31–33], the molecular structure of the title compounds was optimized. Gaussian 09W quantum chemical software was used in all simulated calculations with B3LYP/GEN (C, H, N, Cl: 6-31G(d,p) and Sb: LanL2DZ) [23]. The total and partial density of states (TDOS and PDOS) have been determined to estimate the moieties' contributions to frontier orbitals. Gauss Sum 2.2.1 program generated TDOS and PDOS data are used to determine the contribution of groups to molecular orbitals [24].

The visual technique known as molecular electrostatic potential (MEP) enables us to identify the position of the electron density. A well-known instrument for displaying the reactive behaviors of molecules is the electrical potential: V(r)

$$\mathrm{V(r)} = \sum_A \frac{Z_A}{(R_A - r)} - \int \frac{\rho(r')}{(r' - r)} \mathrm{d}(r') \quad (1)$$

Where $\rho(r')$ is the electronic density function, the nucleus A's charge, called Z_A, is situated at R_A [25–27]. Using theoretical calculations, the map of molecular electrostatic potential was examined to observe and gather information about the molecule's variable-charged areas.

Based on the finite field technique [28], the first static hyperpolarizability (β) and related properties (dipole moment, mean polarizability, and anisotropy of polarizability) have been estimated at the DFT/ B3LYP method and GEN (C, H, N, Cl: 6-31G(d,p) and Sb: LanL2DZ) level.

For the relevant optimized structure, the cartesian coordinates force fields were translated to the internal coordinates [29,30]. Scaled factors were used to scale the elements of the internal force constant matrix (Fij(scaled)) (si and sj).

$$F_{ij}(\text{scaled})=(s_i)^{1/2}F_{ij}(s_j)^{1/2} \quad (2)$$

The scaling factor is required to align each theoretical vibrational frequency with the experimental data. The scaling factors were used from the Computational Chemistry Comparison and Benchmark Database (CCCBDB) and subsequently applied to the obtained vibrational frequencies. The Scaled Quantum Mechanic (SQM) [31] tool was used to scale the quantum mechanical force fields to obtain these internal coordinate forces (Table 1).

For fitting the calculated fundamental wavenumbers to the appropriate experimental, scaled the F=[Fij] matrix was used.

Table 1. Scale factors (si)

Vibrations		Bonds	Final Scale factor
Stretching	1	X-X	1.073
	2	C-H	0.794
	3	Cl-Sb	0.964
	4	N-H	1.043
Bending	5	C-C-H	0.961
	6	C-X-X	1.001
	7	C-N-Sb	1.072
Torsion	8	X-X-X-X	0.887

The merit function χ^2 defines the scaling factor optimization strategy;

$$\chi^2(s_i) = \sum\{[v_i^{exp} - v_i^{theor}(s_i)]w_i\}^2 \quad (3)$$

The percentages of stretching, bending, or torsion that contribute to a specific normal mode were determined by the potential energy distribution (PED).

2.2. Experimental studies

Sigma-Aldrich (USA) was used to purchase all reagents, compounds, and solvents. The synthesis of chlorine and bromine-linked antimony was obtained in this study, as it was synthesized by Tunç et al. in 2016, according to the procedure in previous studies [22]. Synthesis of the complex compounds were done as in the literature [20–22]. In this study, Antimony(III) chloride was dissolved in the same solvent at a mole ratio of 2:1 in hydrochloric acid, and 25 mL of the ligand solution was added. After being refluxed for two days at 60 C, the mixture was concentrated to a third of its original volume and left to stand at room temperature for crystallization. Filters were used to create colorless, yellow, and pink crystals, which were then dried in the air. The syntheses of [1a-3a] complexes were obtained experimentally. The Perkin Elmer Spectrum Two with U-ATR spectrometer was used to observe the Fourier Transform-Infrared Spectra (FT-IR).

3. RESULTS and DISCUSSION

3.1. General Remarks on Geometry

Pyridine and pyrimidine ligands with the formation of SbX_3L_2 (X: Cl and Br, *L^1:2-aminopyridine*, *L^2: 2-amino-5-methylpyridine and L^3: 2-aminopyrimidine*) complexes given in the list below.

[1a]: *[Sb(2-aminopyridine)$_2$Cl$_3$]*
[1b]: *[Sb(2-aminopyridine)$_2$Br$_3$]*
[2a]: *[Sb(5-methyl-2-aminopyridine)$_2$Cl$_3$]*
[2b]: *[Sb(5-methyl-2-aminopyridine)$_2$Br$_3$]*
[3a]: *[Sb(2-aminopyrimidine)$_2$Cl$_3$]*
[3b]: *[Sb(2-aminopyrimidine)$_2$Cl$_3$]*

The geometrical characteristics of Sb-L_2 and Sb-X_3 fragments in the complexes are similar. The atom labelling scheme is shown in Figure 1 and the calculated geometric parameters (bond lengths and angles) are summarized in Table 2. The density functional theory at B3LYP/GEN (C, H, N, Cl: 6-31G(d,p) and Sb: LanL2DZ) was used to thoroughly optimize the ground state structures**.**

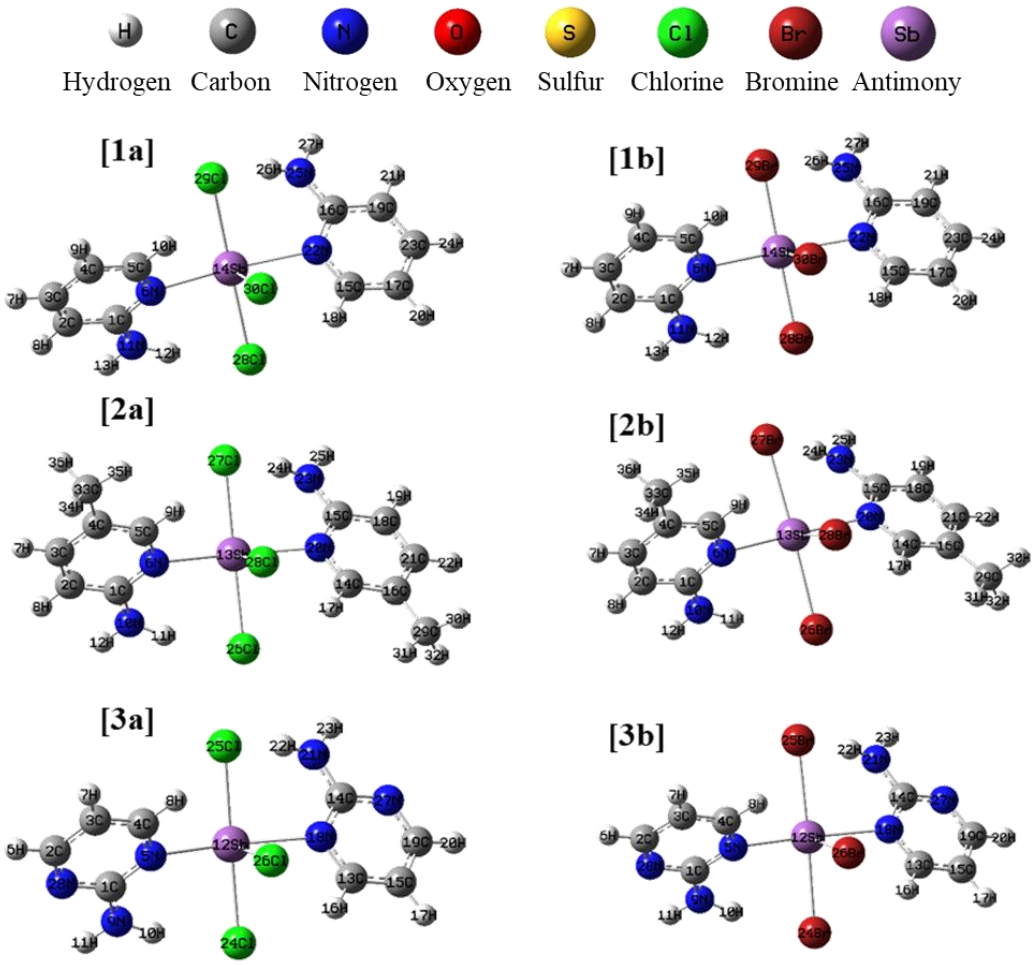

Figure 1. The ground state optimized structure of the complexes.

When we look at the structural parameters of metal halide, Sb-Cl bond length is about 2.66 Å, while Sb-Br bond length is 2.80-2.90 Å. is in the range. All three molecules have a similar structure and trans geometry. The equatorial angles (N-Sb-N) are in varied from 167-172°. Cl-Sb-Cl angle is in the range of 176-179°, planar.

Table 2. Selected calculated structural parameters of the complexes (X = Cl, Br)

R	**[1a]**	**[1b]**	**R**	**[2a]**	**[2b]**	**R**	**[3a]**	**[3b]**
C_1-C_2	1.41	1.42	C_1-C_2	1.42	1.42	C_1-N_5	1.36	1.36
C_1-N_6	1.36	1.35	C_1-N_6	1.37	1.37	C_1-N_9	1.35	1.35
C_1-N_{10}	1.37	1.37	C_1-N_{10}	1.37	1.37	C_1-N_{28}	1.35	1.35
C_2-C_3	1.38	1.38	C_2-C_3	1.39	1.39	C_2-C_3	1.40	1.40
C_2-H_8	1.09	1.09	C_2-H_8	1.09	1.09	C_2-H_6	1.09	1.09
C_3-C_4	1.40	1.42	C_3-C_4	1.42	1.42	C_2-N_{28}	1.33	1.33
N_6-Sb_{14}	2.47	2.49	N_6-Sb_{13}	2.47	2.48	N_5-Sb_{12}	2.47	2.49
Sb_{14}-X_{28}	2.66	2.80	Sb_{13}-X_{26}	2.66	2.91	Sb_{12}- X_{24}	2.65	2.80
Sb_{14}-X_{29}	2.66	2.80	Sb_{13}-X_{27}	2.66	2.91	Sb_{12}-X_{25}	2.65	2.80
Sb_{14}-X_{30}	2.43	2.57	Sb_{13}-X_{28}	2.50	2.68	Sb_{12}-X_{26}	2.43	2.57
(°)	**[1a]**	**[1b]**	**(°)**	**[2a]**	**[2b]**	**(°)**	**[3a]**	**[3b]**
C_7-C_1-N_6	120	120	C_7-C_1-N_6	120	120	N_5-C_1-N_9	119	119
N_6-C_1-N_{11}	119	119	N_6-C_1-N_{10}	119	119	N_9-C_1-N_{28}	117	117
C_1-C_2-C_3	120	120	C_1-C_2-C_3	120	120	C_1-C_2-H_6	121	121
C_5-C_4-H_9	120	120	C_5-C_4-C_{33}	121	121	N_5-C_4-H_8	116	117
C_4-C_5-N_6	123	123	C_4-C_5-N_6	124	124	C_1-N_5-C_4	118	118
N_6-Sb_{14}-X_{28}	92	94	N_6-Sb_{13}-X_{26}	92	93	N_5-Sb_{12}-X_{26}	83	86
N_6-Sb_{14}-X_{29}	87	87	N_6-Sb_{13}-X_{27}	88	87	N_{18}-Sb_{12}-X_{24}	87	94
N_6-Sb_{14}-X_{30}	84	86	N_6-Sb_{13}-X_{28}	84	86	N_{18}-Sb_{12}-X_{25}	93	85
N_{22}-Sb_{14}-X_{28}	88	88	N_{20}-Sb_{13}-X_{26}	88	87	$N_{18}Sb_{12}$-X_{26}	83	92
N_{22}-Sb_{14}-X_{29}	92	92	N_{20}-Sb_{13}-X_{27}	92	93	N_{24}-Sb_{12}-X_{26}	89	92
N-Sb-N	168	172	N-Sb-N	167	172	N-Sb-N	166	170
X-Sb-X	177	179	X-Sb-X	178	176	X-Sb-X	178	179

3.1. Frontier Molecular Orbital Parameters and PDOS

In this section, Frontier molecular orbital parameters and the partial density of state results are given. The highest occupied molecular orbital (HOMO) and lowest unoccupied molecular orbital (LUMO), sometimes known as frontier molecular orbitals, are particularly well-liked quantum chemical characteristics. They determine a molecule's light-absorbing capacity and molecular reactivity. According to Koopmans theorem equations, these descriptors can be expressed as chemical potential $\mu=(E_{HOMO}+E_{LUMO})/2$, chemical hardness $\eta=(E_{HOMO}-E_{LUMO})/2$, global softness $S=1/\eta$ and electrophilicity index $\omega= \mu^2/2\eta$ from the orbital energy gap [32,33].

Table 3 contains a list of descriptors for the antimony (III) compounds [1-3a/b]. Additionally, the table includes information on the anti-leishmanial activity of these compounds. Notably, [3a] exhibits the strongest anti-leishmanial activity among the tested compounds, as evidenced by its highest HOMO value, lowest energy gap, and lowest chemical hardness. The global hardness value is directly related to the stability of the chemical system. [3b] has the highest electrophilicity index (ω).

Table 3. Global reactivity properties and antileishmanial activity

Molecular Properties (eV)	**[1a]**	**[2a]**	**[3a]**	**[1b]**	**[2b]**	**[3b]**
E_{LUMO}	-1.69	-1.62	-2.05	-1.76	-1.69	-2.07
E_{HOMO}	-6.43	-6.23	-6.69	-6.04	-5.97	-6.28
$\Delta E_{HOMO-LUMO}$	-4.74	-4.61	***-4.64***	-4.28	-4.28	-4.21
Ionisation Potential (IP)	6.43	6.23	6.69	6.04	5.97	6.28
Electron Affinity (EA)	1.69	1.62	2.05	1.76	1.69	2.07
Chemical Hardness (η)	2.37	2.31	2.32	2.14	2.14	2.11
Electronegativity (χ)	4.06	3.93	4.37	3.90	3.83	4.18
Chemical Potential (μ)	-4.06	-3.93	-4.37	-3.90	-3.83	-4.18
Softness (S) ev^{-1}	0.42	0.43	0.43	0.47	0.47	0.48
Electrophilicity index (ω)	3.48	3.34	4.12	3.55	3.43	***4.14***
LC_{50} (M)*	$2.19x10^{-5}$	$1.40x10^{-4}$	$1.47x10^{-5}$			

*Antileishmanial activity [34]

The population analysis was calculated and presented in Figure 2. In PDOS plots and the structure of fragment orbitals that are a part of molecular orbitals–demonstrated. Where, the groupings of N-Sb-Cl/Br, Ring, N-H, and other atoms have been divided at the PDOS. A bonding interaction supported the PDOS's positive value, whereas an anti-bonding interaction contends that are negative values and non-binding interactions imply values very near to zero.

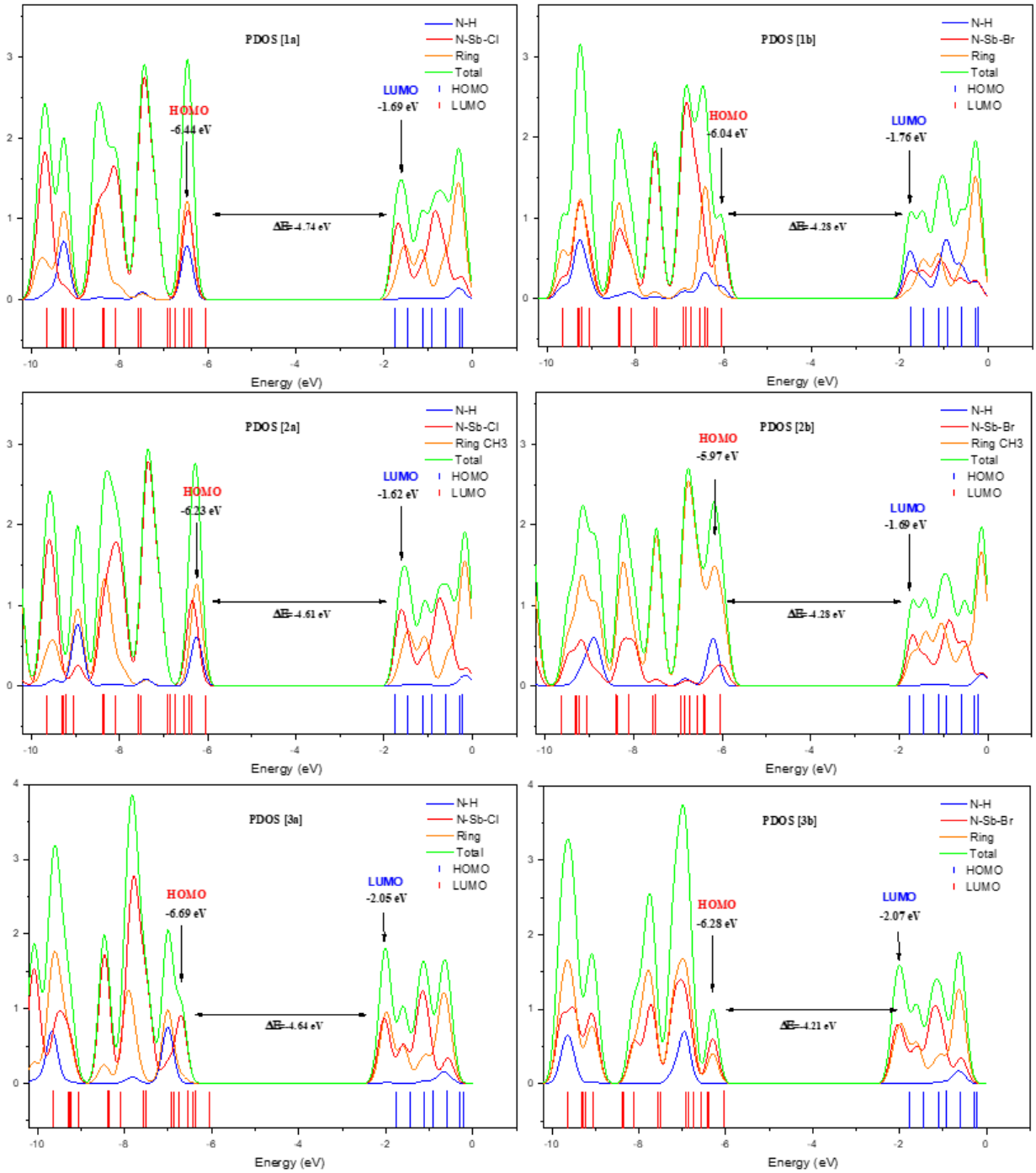

Figure 2. The partial density of state diagrams

As shown in Figure 2, the partial density of state plot (PDOS) primarily illustrates the structure of the fragment orbitals that contribute to the molecular orbitals. The HOMO LUMO orbital distributions of each compound are shown in the graph Figure 2. Table 4 shows the calculated contribution percentages

of the molecular orbitals. The partial density of state plot (PDOS) mainly presents the composition of the fragment orbitals contributing to the molecular orbitals which is seen from Figure 2. The calculated contribution percentage of the structures are listed in Table 4. As seen in the Table 4, HOMO-LUMO orbitals are localized on the N-Sb-X (X=Cl, Br) and their contributions are about 59-90 %.

Table 4. The calculated contribution percentage of the complexes from PDOS

		The contribution percentage			
		eV	N-Sb-Cl	Ring	N-H
[1a]	LUMO	-1.69	81	18	0
	HOMO	-6.43	89	8	3
			N-Sb-Br	Ring	N-H
[1b]	LUMO	-1.76	75	20	5
	HOMO	-6.04	68	26	6
			N-Sb-Cl	Ring CH_3	N-H
[2a]	LUMO	-1.62	81	18	0
	HOMO	-6.23	62	30	8
			N-Sb-Br	Ring CH_3	N-H
[2b]	LUMO	-1.69	61	38	0
	HOMO	-5.97	59	41	0
			N-Sb-Cl	Ring	N-H
[3a]	LUMO	-2.05	65	35	0
	HOMO	-6.69	90	9	1
			N-Sb-Br	Ring	N-H
[3b]	LUMO	-2.07	78	12	0
	HOMO	-6.28	60	40	0

3.2. Molecular Electronic Potential Surface

A method for illustrating the distribution of electrostatic potential is the molecular electrostatic potential (MEP) surface. Different colours are used to represent the various electrostatic potential levels at the surface. Potential increases from red-orange-yellow-green-blue, with blue denoting the highest electrostatic potential energy and red denoting the lowest. Molecular electrostatic potential (MEP) provide the distribution, molecular structure, size, and dipole moments of the complexes, and allowing the reader to comprehend electrophilic attack and nucleophilic interactions. In Figure 3, the negative (red) portions of MEP were linked to electrophilic reactivity, whereas the positive (blue) regions were linked to nucleophilic reactivity. The negative (red) and positive (blue) regions of MEP were connected to electrophilic and nucleophilic reactivity, respectively. According to Figure 3, there are two possible targets for electrophilic attack on complex compounds, negative areas are mostly around N-Sb-X (X: Cl, Br), while the positive ones around the nitrogen atoms.

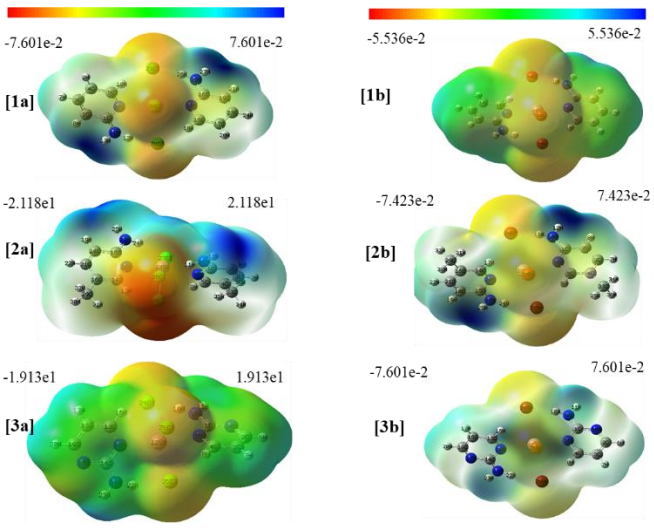

Figure 3. Molecular electronic potential surface of the complexes

3.3. First Hyperpolarizability

For emerging technologies in fields like communication, signal processing, and optical interconnections, such as frequency shifting, optical modulation, switching, and logic, nonlinear optical (NLO) activity provides essential functions [35,36]. The first hyperpolarizability of a system in the presence of an applied electric field is a third-rank tensor that may be characterized by a 3x3x3 matrix, and the energy of a system is a function of the electric field. Using the x, y, and z components, the total static dipole moment (μ), mean polarizability ($<\alpha_{tot}>$), anisotropy of polarizability (Δα), and first-order hyperpolarizability (β_{tot}) can be determined as follows:

$$\mu = (\mu_x^2 + \mu_y^2 + \mu_z^2)^{1/2} \quad (4)$$

$$<\alpha_{tot}> = 1/3\ (\alpha_{xx} + \alpha_{yy} + \alpha_{zz}) \quad (5)$$

$$\Delta\alpha = 2^{-1/2}[(\alpha ii-\alpha jj)^2+(\alpha ii-\alpha kk)^2+(\alpha jj-\alpha kk)^2+6\alpha xx^2]^{1/2} \quad (6)$$

$$\beta_i = (\beta_{iii} + \beta_{ijj} + \beta_{ikk}) \text{ and } i, j, k = x, y, z \quad (7)$$

$$\beta_{tot} = (\beta_x+\beta_y+\beta_z)^{1/2} \quad (8)$$

With the calculating by using the schemes of the B3LYP/GEN value of electric dipole moment, polarizabilities and first hyperpolarizabilities for the title complexes were tabulated in Table 5 ($\Delta\alpha_{tot}\times10^{-23}$ esu and $\beta_{tot}\times10^{-31}$ esu). αi, β_{ikk} components of the polarizability and first hyperpolarizability can be seen in Table S1 (Supplementary Information). Since the polarizabilities and hyperpolarizabilities of the Gaussian 03 outputs are presented in atomic units (a.u.), the predicted values have been transformed into electrostatic units by using α: 1a.u. = 0.1482×10^{-24} esu and β; 1a.u. = 8.6393×10^{-33} esu, respectively. Along the z-axis, the highest dipole moment was identified for all complexes. Among the complexes, the largest dipole moment is μ=10.77 Debye [2b] and the lowest molecular dipole moment is μ=0.25 Debye [3b]. At the same time [3b] complex has β_{tot}=241.85 a.u. and it has a relatively higher average polarizability Δα (a.u.) value than the others. x, y, and z components of dipole (μ), polarizability (α), and first-order hyperpolarizability (β) were given in the Table S1 (Supplementary information).

Table 5. The calculated dipole moment, polarizabilities and first-order hyperpolarizabilities of the complexes

μ&α	**[1a]**	**[2a]**	**[3a]**	**[1b]**	**[2b]**	**[3b]**
μ (Debye)	1.24	1.02	0.64	1.13	10.77	0.25
<α> (a.u.)	216.33	243.56	207.36	240.49	473.20	231.43
Δα (×10^{-23} esu)	7.73	8.60	7.40	8.19	21.40	7.86
βx	6.03	2.15	-0.63	-3.22	2.84	-7.37
βy	-8.12	-10.79	-5.01	-3.99	-0.07	-0.39
βz	15.76	24.63	115.98	105.06	-1851.43	241.73
β_{tot} (a.u.)	18.73	26.98	116.09	105.19	1851.44	241.85
βtot (×10^{-31} esu)	1.62	2.33	10.03	9.09	159.95	20.89

α (1 a.u.) = 0.1482×10^{-24} esu; β (1 a.u.) = 8.6393×10^{-33} esu

Table S1. x, y, and z components for dipole (μ), polarizability (α), and first-order hyperpolarizability (β)

μαβ	**[1a]**	**[2a]**	**[3a]**	**[1b]**	**[2b]**	**[3b]**
μx	1.00E-07	-1.90E-06	2.20E-06	1.48E-05	2.79E-05	1.19E-05
μy	4.30E-06	7.70E-06	-5.10E-06	-1.16E-05	8.19E-05	3.00E-06
μz	-1.24	-1.02	-0.45	-1.13	-10.77	-0.25
αxx	292.32	326.24	279.32	311.69	786.73	298.55
αxy	-16.48	-16.98	-19.28	-18.80	70.06	-22.13
αyy	207.55	228.73	206.32	235.56	362.80	233.35
αxz	0.00	0.00	0.00	0.00	0.00	0.00
αyz	0.00	0.00	0.00	0.00	0.00	0.00

αzz	149.11	175.70	136.44	174.23	270.07	162.39
βxxx	0.67	-0.78	-0.38	-2.81	0.93	-0.94
βxxy	-2.15	-3.12	-2.89	-0.34	0.49	0.09
βxyy	3.14	4.80	-1.92	0.18	0.67	-2.74
βyyy	-7.06	-6.89	-1.58	-2.49	0.65	1.07
βxxz	-2.72	28.97	86.18	46.61	512.11	153.95
βxyz	135.92	-119.45	-111.91	-139.97	-829.97	-115.28
βyyz	136.47	76.27	148.80	181.00	-1592.29	193.04
βxzz	2.22	-1.87	1.67	-0.59	1.24	-3.69
βyzz	1.08	-0.77	-0.54	-1.16	-1.21	-1.56
βzzz	-117.99	-80.61	-118.99	-122.55	-771.25	-105.25

3.4. Vibrational Spectral Analysis

The title compound's vibrational frequencies were made, and the calculated results were contrasted with experimental FT-IR spectra in this section. The scaled quantum mechanical force field (SQM-FF) methodology has been applied to the theoretically anticipated wavenumbers using the SQM program. Depending on the type of Hessian calculations, it is expected that the harmonic wavenumbers estimated for a molecule will greatly exceed the corresponding actual wavenumbers. The SQM-FF method, which applies an effective empirical scaling process to the calculated harmonic wavenumbers or, more preferably, to the calculated harmonic force constants, can successfully correct these overestimations even though they are not completely systematic [27, 28]. These findings suggest that the calculated expected frequencies match the observed infrared values quite well. According to the SQMFF technique, the average percentage error RMS was found to be 11.09, 12.64, and 14.26 for the [1a-3a] complexes, respectively (see Table 6).

Table 6. RMS values of SQM calculation

	[1a]	**[2a]**	**[3a]**
RMS error	11.09	12.64	14.26
Pre-fingerprint region	4.51	1.59	12.71
Fingerprint region (500-2500 cm^{-1})	12.60	11.69	15.62
Post-fingerprint region	2.35	16.55	11.30

Total Energy Distribution (TED), which is produced by the SQMFF technique, was used to create characterized normal mode descriptions and interpret them. The TED components quantify the contribution of each internal coordinate to the external coordinates. The descriptions of the internal coordinates utilized in the TED computations are provided in Table S2-S4. Experimental and calculated-SQM infrared spectrums of the complexes [1a-3a] shown in the Figure 4, 5 and 6.

Table S2. The vibrational wavenumbers, harmonic and scaled (SQM) frequencies (cm−1), IR intensities, TED and assignments of [1a]

		B3LYP		SQM		Exp.	
No		$Freq^{Har}$	I_{IR}	$Freq^{SQM}$	I_{IR}^{SQM}	IR^{Exp}	Mode Description and TED>%5
1	A	27	1.25	26	1.4		τHClClH(52)+τSbClHN(28)+δClSbN(12)+δClHN(12)
2	A	28	4.08	28	4.1		τSbClHN(36)+τHClClH(71)
3	A	40	2.28	40	2.3		τSbClHN(242)+τHNCC(16)
4	A	46	0.28	46	0.3		τSbClHN(135)+δClHN(28)+δHNC(11)
5	A	71	1.15	70	1.1		τHClSbCl(60)+τSbClHN(58)+δSbClH(16)
6	A	85	1.20	84	1.1		τClHNC(78)+tClHNH(145)+tHNCN(88)
7	A	97	3.31	97	3.4		δHNCl(52)+δSbClH(14)+τSbClHN(50)
8	A	113	4.14	112	3.5		δHClSb(52)+τClHNC(50)+τClHNH(32)+τHClSbCl(20)
9	A	123	39.13	121	0.4		δSbClH(65)+τHNCN(26)
10	A	125	0.66	123	44.6		νClH(64)+δHClSb(30)+δClSbCl(13)+τSbClNH(27)
11	A	135	18.12	133	13.8		δClHN(76)+τClSbCl(27)
12	A	136	0.42	135	0.2		νClH(83)+νHSb(11)+τClHNC(62)+τClHNH(40)
13	A	141	14.31	143	14.5		νClH(83)+νHSb(11)+τClHNC(62)+τClHNH(40)
14	A	171	0.11	170	101.8		νSbCl(17)+νSbH(15)+τHClSbCl(25)+τClHNC(12)+τClHNH(11)
15	A	172	108.82	171	0.4		δClHN(27)+τClHNC(164)+τClHNH(119)+τHCLCLH(9)
16	A	216	43.30	210	29.7		νClSb(11)+τCCCN(18)+τCNCN(10)+τClHNC(15)

17	A	220	2.84	216	2.8			νClSb(30)+τCCCN(14)+τSbClHN(30)
18	A	235	0.55	233	0.0			νClSb(31)+νClH(15)+τSbClHN(26)
19	A	241	88.27	240	104.9			νClSb(69)+νClH(11)
20	A	313	30.63	318	28.7			νClSb(95)
21	A	430	16.98	405	17.0			δCCN(36)
22	A	433	10.09	409	5.4			δCCC(16)+δCCN(16)+τSbClHN(16)
23	A	437	26.99	432	22.0			δNCC(62)+τClHNH(13)
24	A	438	2.37	434	10.9			δCCN(30)+δCNC(25)+τClHNH(36)
25	A	475	26.42	458	32.5			τHNCN(22)+τHNCN(20)+τClHNH(36)+τClHNC(11)
26	A	479	88.01	461	96.5			δNCC(11)+τHNCC(21)+τHNCN(21)
27	A	529	7.90	501	8.7	496	m	τRing(54)
28	A	529	29.63	501	24.0			τRing(54)
29	A	571	0.28	558	2.3	549	w	δCCN(22)
30	A	572	13.14	559	16.8			δCCN(22)+τClHNC(25)+τClHNH(15)
31	A	652	73.29	646	145.4	626	m	τSbClHN(100)
32	A	653	33.11	648	199.3			τSbClHN(100)
33	A	659	78.11	654	1.0	653	m	τClHNC(22)
34	A	663	250.82	656	72.6			βCCC(13)+τClHNC(28)+τSbClHN(76)
35	A	755	10.70	720	13.3	719	w	τRing(44)+τSbClHN(13)
36	A	756	0.07	721	8.1			τCCCH(15)+τCNCC(15)+tHCCN(14)+tSbClHN(13)
37	A	781	39.69	749	37.2			τCCCH(48)+τHCCN(25)
38	A	782	77.09	749	74.0	763	m	τCCCH(48)+τHCCN(25)
39	A	862	22.09	824	45.0			νCN(53)+νCC(8)+δCCC(13)
40	A	864	1.11	827	0.0			νCN(53)+νCC(8)+δCCC(13)
41	A	864	6.35	831	2.8			τCCCH(14)+τHCCH(13)+τHCCN(18)
42	A	864	4.51	831	8.4			τCCCH(14)+τHCCH(13)+τHCCN(18)
43	A	973	0.04	916	0.0			τHCCH(46)+τHCCC(18)+τHCCC(16)
44	A	974	0.25	917	0.4			τHCCH(46)+τHCCC(18)+τHCCC(16)
45	A	1004	0.52	949	0.1			τHCCH(74)
46	A	1004	0.12	949	0.4			τCCCH(25)+τHCCH(48)
47	A	1016	75.62	987	116.5			δCNC(34)+νCN(29)
48	A	1018	0.68	991	1.2	993	w	δCNC(34)+νCN(29)
49	A	1081	29.26	1082	7.0			δHNC(36)+νCC(17)
50	A	1082	0.33	1083	0.0			δHNC(33)+νCC(17)
51	A	1085	1.46	1096	0.3			νCC(50)ring
52	A	1085	0.00	1097	0.0	1119	w	νCC(50)ring
53	A	1166	1.72	1150	13.8			νCN(25)+δHCC(25)
54	A	1167	2.20	1151	0.0	1164	w	νCN(15)+δHCC(28)
55	A	1190	17.33	1193	16.2			δHCC(76)
56	A	1190	8.78	1193	11.8	1190	w	δHCC(76)
57	A	1320	71.61	1252	55.5	1234	w	νCN(29)+νCC(23)
58	A	1322	1.95	1254	0.0			νCN(29)+νCC(23)
59	A	1371	42.30	1318	55.1			νCN(54)+νCC(12)
60	A	1371	10.59	1318	27.8	1321	m	νCN(54)+νCC(12)
61	A	1382	1.08	1370	31.0			δNCH(22)+δHCC(15)+δHNC(15)
62	A	1383	0.08	1370	5.8	1382	m	δNCH(22)+δHCC(15)+δHNC(15)
63	A	1494	60.56	1483	85.7	1472	m	δCCH(27)+νCC(15)
64	A	1495	37.61	1483	58.3			δCCH(28)+νCC(14)
65	A	1539	97.31	1525	84.7			δHCN(28)+δHCC(18)
66	A	1541	68.43	1527	58.1	1544	m	δHCN(28)+δHCC(18)
67	A	1621	74.78	1632	57.7	1621	s	νCC(54)
68	A	1621	25.26	1632	16.4			νCC(54)
69	A	1667	136.36	1674	122.2	1661	s	δHCH(49)+δHCH(17)
70	A	1668	0.65	1675	25.7			δHCH(49)+δHCH(17)
71	A	1697	259.89	1697	37.3			νCC(36)+νCN(21)
72	A	1698	88.21	1698	205.1			νCC(36)+νCN(21)
73	A	3195	8.76	3138	9.3			νHC(98)
74	A	3195	2.78	3138	2.4			νHC(98)
75	A	3210	23.61	3153	23.5			νHC(95)
76	A	3210	4.04	3153	4.0			νHC(94)
77	A	3228	0.43	3170	0.4	3169	m	νHC(95)
78	A	3228	1.80	3170	1.6			νHC(95)
79	A	3241	0.75	3183	0.7			νHC(97)
80	A	3241	15.21	3183	14.7	3184	m	νHC(97)
81	A	3416	722.76	3346	722.0	3343	s	νHN(96)
82	A	3416	11.43	3347	11.6			νHN(96)
83	A	3670	104.88	3597	104.8			νHN(95)

84	A	3671	33.51	3597	33.3	3600	m	νHN(95)

[Har] Harmonic vibrational frequencies. Freq[SQM], Calculated from SQM frequencies, I[IR] Infrared intensities
ν, stretching; δ, bending; τ, torsion.

Table S3. The vibrational wavenumbers, harmonic and scaled (SQM) frequencies (cm^{-1}), IR intensities, TED and assignments of [2a]

		B3LYP		SQM		Exp.		
No		Freq[Ha]	I_{IR}	Freq[SQ]	I_{IR}^{SQM}	IR[Exp]		Mode Description and TED>%5
1	A	26	0.85	24	0.86			τSbClHN(84)
2	A	29	4.10	28	4.10			τSbClHN(100)
3	A	34	0.00	34	0.00			τSbClHN(81)+δHClSb(23)+δClHN(23)
4	A	35	2.60	35	2.57			τSbClHN(217)+δHClSb(17)
5	A	70	0.53	69	0.44			τSbClHN(95)+τHClSbCl(11)+δHClSb(17)
6	A	79	0.40	78	0.33			τClHNC(170)+τClHNH(151)
7	A	88	0.04	85	0.08			τHCCC(62)+τClHNH(27)+τClHNC(32)
8	A	88	0.58	85	0.32			τHCCC(84)
9	A	91	3.49	90	3.87			δClHN(68)+τSbClHN(29)+τClHNH(28)
10	A	106	3.51	105	3.29			νClH(14)+δSbClH(31)+τClHNC(29)+τHClSbCl(26)
11	A	116	18.12	114	16.23			δClHN(22)+τHClSbCl(20)
12	A	118	0.04	116	0.02			δHClSb(79)+τHNCN(13)
13	A	122	0.14	121	0.05			τClHNC(82)+τClHNH(62)+νClH(22)+δClHN(20)
14	A	125	42.10	125	46.43			νClH(41)+δSbClH(25)+δClHN(12)+τSbClHN(39)
15	A	140	18.68	142	17.74			δClSbCl(61)+δHClSb(22)
16	A	152	0.21	151	0.31			νClH(64)+τClHNC(46)+τClHNH(41)
17	A	154	9.64	153	6.34			νClH(14)+νSbCl(11)+δClSbCl(18)+τSbClHN(15)
18	A	168	3.47	166	2.86			τClHNC(69)+τClHNH(40)
19	A	175	93.96	174	91.88			δClH(11)+τClHNC(18)+τHClSbCl(43)
20	A	224	123.19	226	122.14			νClSb(84)
21	A	224	0.63	227	0.76			νClSb(88)
22	A	309	25.23	310	11.54			νClSb(39)+δCCC(29)
23	A	319	27.76	312	25.80			δCCC(48)+τClHNC(19)+τClHNH(17)
24	A	321	3.63	315	1.27			δCCC(10)+τCCCC(12)+τCCCN(5)
25	A	324	0.82	315	4.41			τCCCC(12)+τCCCN(13)
26	A	325	0.78	320	15.68			νClSb(53)+δCCC(10)+tClHNC(44)+τClHNH(32)
27	A	438	12.91	424	14.40	422	w	τCC/NCC(18)+τSbClHN(11)
28	A	442	9.91	428	3.30			τCCCC(13)+τCNCC(17)+τSbClHN(30)
29	A	450	5.05	439	7.56			δCCN(40)+τHNCC(10)+τClHNH(14)
30	A	451	12.86	440	19.49			δCCN(21)+δNCN(15)+τClHNH(35)
31	A	469	39.97	458	32.59			δCCN(13)+τHNCC(17)+tHNCN(14)
32	A	472	67.53	460	69.58			δCCN(13)+τHNCC(17)+tHNCN(14)
33	A	490	5.21	475	9.67			νCC(10)+δNCN(15)+δCCC(13)+δCCC(11)
34	A	490	2.61	476	6.67	477	m	νCC(10)+δNCN(15)+δCCC(24)
35	A	531	6.53	515	6.76	512	m	τRing(33)
36	A	531	30.57	516	26.50			τRing(33)
37	A	656	144.92	647	146.98	645	w	τSbClHN(149)
38	A	660	290.84	650	233.11			τSbClHN(163)
39	A	676	5.27	660	1.08			τRing(45)+τSbClHC(33)
40	A	678	30.79	662	84.91			τClHNC(69)+τClHNH(10)
41	A	754	4.65	732	3.29			νCC(21)+δCCN(14)
42	A	754	8.57	732	6.76	740	w	νCC(21)+δCCN(14)
43	A	787	29.97	763	29.76	757	w	SbClHN(45)
44	A	789	6.81	764	14.93	789	w	τSbClHN(64)
45	A	834	22.97	817	22.16			τHCCN(60)
46	A	834	49.00	817	49.18	829	w	τHCCN(57)
47	A	874	42.42	835	59.77			νCC(29)+νCN(27)
48	A	877	0.09	838	0.00			νCC(29)+νCN(27)
49	A	923	1.17	895	0.90			τHCCC(60)
50	A	924	0.80	896	0.54			τHCCH(45)
51	A	990	0.03	961	0.01			τHCCH(61)
52	A	990	0.29	961	0.46			τHCCH(55)
53	A	1014	1.00	984	2.54			δHCC(31)
54	A	1014	0.00	984	0.01			δHCC(31)
55	A	1060	44.25	1030	59.36			δNCC(11)
56	A	1060	0.35	1030	0.41	1030	w	δNCC(11)
57	A	1073	2.34	1043	2.40			δHCC(62)
58	A	1073	3.57	1043	3.55	1054	w	δHCC(62)

59	A	1107	60.37	1082	49.28			δHNC(40)
60	A	1109	0.02	1084	0.01			δHNC(42)
61	A	1179	23.41	1147	31.10			δCCH(57)
62	A	1180	11.10	1148	11.99	1148	m	δCCH(56)
63	A	1253	19.79	1204	41.51	1212	w	νCC(38)
64	A	1254	0.12	1206	0.01	1230	w	νCN(30)+νCC(27)
65	A	1325	52.91	1258	26.01			νNC(48)+νCC(22)
66	A	1326	6.37	1259	1.29			νNC(48)+νCC(26)
67	A	1369	15.23	1311	19.42			νNC(40)+νCC(25)
68	A	1370	2.09	1312	5.91	1319	w	νNC(40)+νCC(25)
69	A	1377	32.19	1344	31.59	1342	m	δHNC(47)+δHCC(15)
70	A	1379	4.39	1345	4.59			δHNC(36)+δHCC(15)+δHNC(11)
71	A	1435	10.80	1397	95.73	1385	m	δHCH(48)
72	A	1435	2.35	1397	59.90			δCC(26)
73	A	1448	55.81	1418	2.16	1414	m	δCCC(95)
74	A	1448	29.74	1418	0.35			δCCC(95)
75	A	1499	4.06	1480	3.88	1455	m	δHCH(56)+δHCC(16)
76	A	1499	6.15	1480	5.94			δHCH(56)+δHCC(16)
77	A	1512	14.82	1490	18.64			δHCH(31)+δHCC(17)
78	A	1512	14.95	1490	18.09			δHCH(31)+δHCC(17)
79	A	1555	143.26	1500	137.26			νNC(22)
80	A	1557	104.17	1502	97.81			νNC(23)
81	A	1617	90.49	1566	85.16	1550	s	νCC(27)
82	A	1618	13.58	1567	6.70			νCC(27)
83	A	1675	83.45	1630	2.12	1624	s	νCC(25)
84	A	1675	3.23	1631	84.24			νCC(25)
85	A	1699	223.89	1658	174.43			δHNH(54)
86	A	1700	81.27	1660	60.88	1667	s	δHNH(52)
87	A	3044	53.54	3027	54.05			νHC_3(81)svm
88	A	3044	17.24	3028	17.24	3040	w	νHC_3(81)svm
89	A	3099	14.90	3082	17.01			νHC_3(100)assym
90	A	3099	16.53	3082	14.42	3090	w	νHC_3(100)assym
91	A	3136	12.88	3119	14.10			νHC_3(82)assym
92	A	3136	4.98	3119	3.82			νHC_3(81)assym
93	A	3184	21.17	3167	23.19	3155	m	νHC(93)
94	A	3184	1.25	3167	1.19			νHC(92)
95	A	3206	18.74	3188	18.03	3181	m	νHC(99)
96	A	3206	5.95	3188	5.86			νHC(99)
97	A	3222	0.22	3204	0.25			νHC(99)
98	A	3222	19.04	3205	17.06	3261	m	νNH(99)
99	A	3418	725.81	3265	726.33	3296	m	νHN(94)
10	A	3418	8.39	3266	8.58	3414	m	νHN(93)
10	A	3668	98.66	3506	98.19	3482	m	νHN(93)
10	A	3669	32.74	3506	32.70			νHN(93)

[Har] Harmonic vibrational frequencies. $Freq^{SQM}$, Calculated from SQM frequencies, I^{IR} Infrared intensities
ν, stretching; δ, bending; τ, torsion.vw, very weak; w, weak; m, medium; s, strong; vs, very strong.

Table S4. The vibrational wavenumbers, harmonic and scaled (SQM) frequencies (cm^{-1}), IR intensities, TED and assignments of [3a]

		B3LYP		SQM		Exp.	
No		$Freq^{Har}$	I_{IR}	$Freq^{SQM}$	I_{IR}^{SQM}	IR^{Exp}	Mode Description and TED>%10
1	A	21	1.03	19	1.10		τSbClHN(26)+τHClSbCl(34)+τHClClH(71)
2	A	26	0.93	26	0.95		δClHN(24)
3	A	43	0.98	42	0.99		δClHN(34)+τSbClHN(120)
4	A	43	1.31	43	1.34		τSbClHN(203)
5	A	73	1.95	72	1.83		τHClClH(17)
6	A	84	2.44	84	2.51		δHClSb(31)+τClHNC(62)+τClHNH(80)
7	A	96	2.49	96	2.56		τSbClHN(56)
8	A	112	4.01	111	3.48		δHClSb(104)+τClHNC(46)
9	A	120	0.11	118	0.05		δHClSb(89)+τClHNC(27)+τClHNH(48)
10	A	124	39.74	124	43.56		δClSbCl(72)
11	A	129	14.48	128	14.11		δClHN(47)
12	A	134	0.01	134	0.00		νClH(58)+δHClSb(28)
13	A	141	19.81	143	18.22		νClH(48)+δClHN(48)+τClHNC(24)
14	A	167	81.19	167	71.23		νClH(20)

15	A	170	1.90	169	2.42			νClH(45)
16	A	207	39.04	203	42.11			τSbClHN(109)
17	A	215	4.29	211	3.50			τSbClHN(109)
18	A	230	0.00	232	0.26			νClSb(84)+τSbClHN(38)
19	A	238	112.46	240	114.63			νClSb(92)
20	A	315	28.94	319	27.56			νClSb(94)
21	A	427	8.47	413	9.85			τCNCC(36)
22	A	430	6.35	417	5.29			τCNCC(89)
23	A	453	80.42	450	80.22	433	w	δNCN(60)+δClHN(30)
24	A	455	3.63	452	4.11	458	m	δNCN(44)+δClHN(50)
25	A	521	5.38	503	5.77	503	m	τNCCC(33)+τHCCC(14)
26	A	522	49.56	503	45.12			τNCCC(26)+τHCCC(26)
27	A	560	0.24	544	0.01	547	w	τHNCN(67)
28	A	563	195.89	546	179.02			τHNCN(68)
29	A	596	6.51	589	9.35			τClHNC(31)+τClHNH(16)
30	A	596	4.65	589	13.46	582	w	τClHNC(33)+τClHNH(18)
31	A	634	83.35	627	80.80			τSbClHN(187)+τHNCN(33)
32	A	637	165.50	629	177.70	640	m	τSbClHN(184)
33	A	662	49.28	657	43.25			δCNC(66)
34	A	664	1.50	659	1.25			δCNC(65)
35	A	802	28.47	778	32.20	777	m	τCNCN(28)
36	A	803	54.61	779	63.56			τHNCN(28)
37	A	813	7.15	798	3.60	792	m	τNCCC(23)+τNCNC(14)
38	A	814	11.06	798	3.52			τNCCC(23)+τNCNC(14)
39	A	890	38.12	864	41.44			νNC(65)
40	A	892	0.06	867	0.04	870	vw	νNC(65)
41	A	988	0.11	952	0.08			τHCCH(21)+τCCCH(22)
42	A	988	0.29	952	0.19			τHCCH(22)+τCCCH(22)
43	A	1009	3.18	973	0.60			τCCCH(35)+τHCCH(22)+tCNCH(20)
44	A	1009	0.15	973	0.13			τCCCH(35)+τHCCH(22)+tCNCH(20)
45	A	1014	8.63	994	8.53	988	m	νCC(6)+δCCC(10)
46	A	1015	0.46	995	0.06			νCC(6)
47	A	1062	32.97	1039	22.96			δHNC(26)+νNC(18)+νCC(15)
48	A	1063	0.15	1040	0.03	1045	vw	δHNC(26)+νNC(18)+νCC(15)
49	A	1113	7.66	1065	6.73			νCC(46)+νCN(10)
50	A	1114	1.76	1066	1.60	1067	vw	νCC(46)+νCN(10)
51	A	1162	3.47	1141	19.82	1115	m	δHCC(42)+νCC(14)
52	A	1163	0.25	1142	1.69	1196	w	δHCC(42)+νCC(13)
53	A	1283	78.79	1235	99.91	1213	m	νNC(67)+νCC(12)
54	A	1284	5.79	1236	7.90			νNC(66)+νCC(12)
55	A	1348	45.49	1338	49.82			δHNC(59)
56	A	1349	0.00	1339	0.00	1344	m	δHNC(57)
57	A	1402	61.87	1375	55.21			νCN(49)+δHCN(17)
58	A	1403	12.21	1376	11.71	1386	m	νCN(46)+δHCN(17)
59	A	1489	7.04	1468	10.06	1450	m	δHCC(53)+νCN(11)
60	A	1491	0.66	1470	0.01			δHCC(52)+νCN(11)
61	A	1526	172.25	1494	214.63			νNC(45)
62	A	1526	90.24	1494	109.55	1509	m	νNC(43)
63	A	1608	279.23	1547	301.71	1540	s	νCC(31)+νCN(15)
64	A	1609	59.69	1548	52.63			νCC(31)+νCN(15)
65	A	1653	188.38	1607	24.33			νCN(39)+νCC(14)
66	A	1654	0.03	1607	227.65	1620	s	νCN(39)+νCC(14)
67	A	1689	500.18	1667	372.02			δHNH(59)+νNH(13)
68	A	1689	160.76	1669	122.90	1660	vs	δHNH(59)+νNH(13)
69	A	3174	54.43	3127	54.51			νHC(99)
70	A	3174	0.35	3127	0.40	3145	m	νHC(99)
71	A	3225	0.00	3177	0.00	3160	m	νHC(93)
72	A	3225	9.31	3177	9.51			νHC(92)
73	A	3248	5.35	3199	4.80	3198	m	νHC(97)
74	A	3248	0.48	3199	0.68			νHC(97)
75	A	3442	205.37	3350	666.03	3347	m	νHN(94)
76	A	3442	462.15	3350	2.56			νHN(94)
77	A	3684	224.00	3586	223.57			νHN(93)
78	A	3684	50.95	3586	50.99	3589	w	νHN(93)

[Har] Harmonic vibrational frequencies. Freq[SQM], Calculated from SQM frequencies, I[IR] Infrared intensities
ν, stretching; δ, bending; τ, torsion.vw, very weak; w, weak; m, medium; s, strong; vs, very strong.

3.4.1. NH_2 Group Vibrations

The N–H stretches of primary aliphatic amines in the region of 3450-3160 cm^{-1}, give rise to two asymmetric and one symmetric stretching vibration. The νNH_2 vibration medium band was assigned at 3600 cm^{-1} and 3343 cm^{-1} [1a]. The corresponding calculated asymmetric and symmetric νNH_2 vibrations were found at 3597 cm^{-1}, 3346 cm^{-1} , and 3296 cm^{-1} in [1a] compound. In compound [2a], NH stretching vibration were observed as 3482 cm^{-1}, 3414 cm^{-1} and 3296 cm^{-1}, calculated 3506 cm^{-1}, 3266 cm^{-1} and 3265 cm^{-1}. In compound [3a], νNH_2 bands were observed at 3589 cm^{-1} and 3347 cm^{-1} and were calculated at 3589 cm^{-1} and 3350 cm^{-1}.

3.4.2. Aromatic C-H and CH_3 Group Vibrations

The characteristic aromatic and heteroaromatic C-H stretching vibrations are expected to appear in the wavenumber range 3000–3200 cm^{-1} [37,38]. The C-H stretching vibrations of the [1a] were observed at 3184, 3169 cm^{-1} in the FT-IR spectrum and calculated as 3183 cm^{-1} and 3170 cm^{-1}. C-H bands were [1] assigned 3181 3155 3090 3040 cm^{-1} assigned of number [2a] compounds. νHC vibrations were assigned experimental at 3198 cm^{-1}, 3145 cm^{-1} and calculation at 3199 cm^{-1}, 3177 cm^{-1} in [3a].
Fundamental $\nu(CH_3)$ stretching symmetric and asymmetric bands appear in the range 3090, 3040 cm^{-1} corresponding to the SQM frequencies 3119 cm^{-1}, 3082 cm^{-1}, and 3028 cm^{-1} respectively for the [2a]th compound because only [2a] has CH_3 group.

3.4.3. Sb-Cl Vibrations

Sb-Cl vibrations were calculated 216, 233, 240, and 318 cm^{-1} for [1a], 226, 227, and 310 cm^{-1} for [2a] and 232, 240 and 319 cm^{-1} for [3a]. 280 cm^{-1} and 308 cm^{-1} for νSbCl in the literature [39].

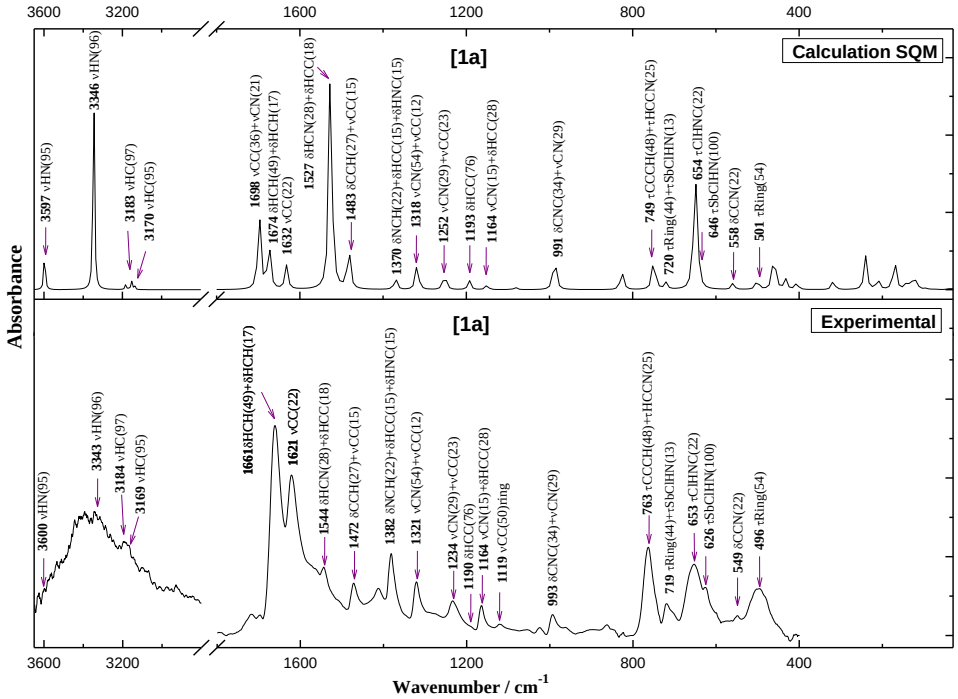

Figure 4. The experimental and simulated infrared spectrum of the complex [1a]

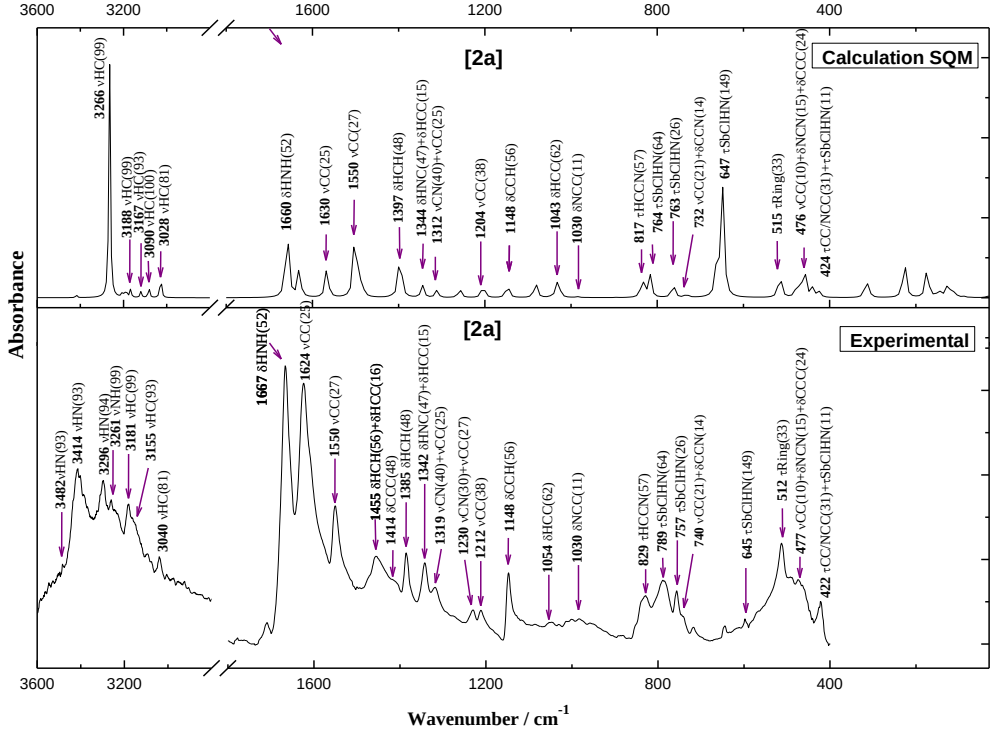

Figure 5. The experimental and simulated infrared spectrum of the complex [2a]

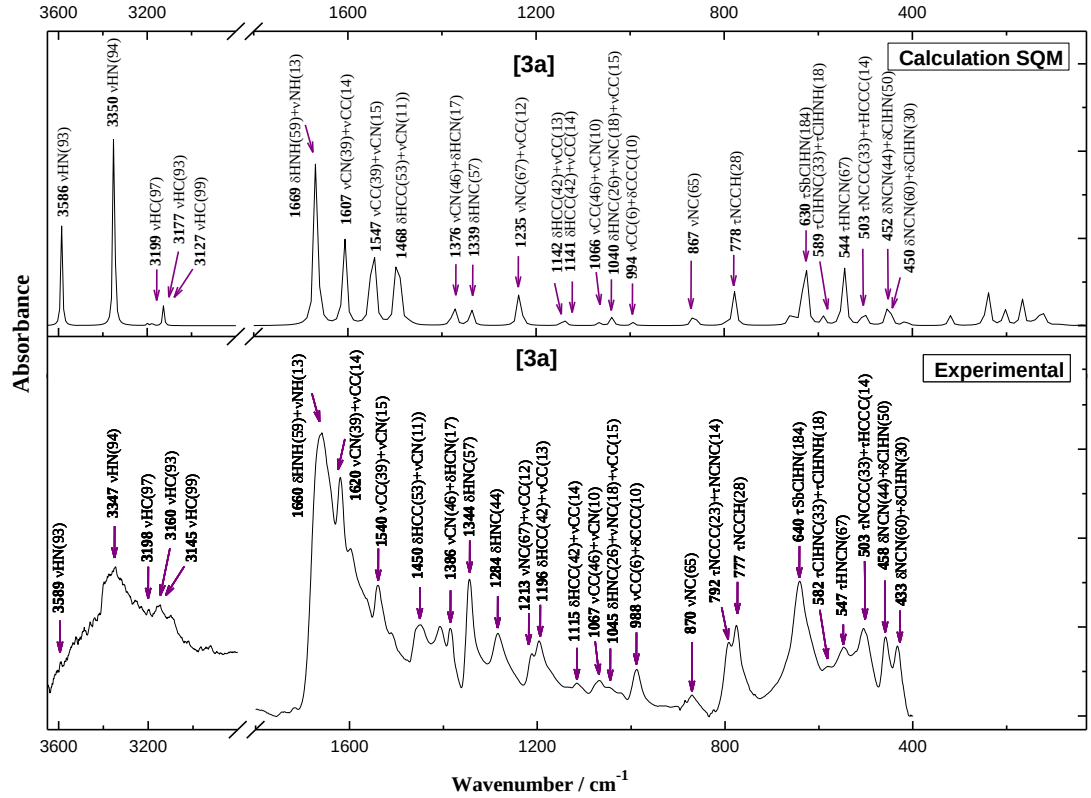

Figure 6. The experimental and simulated infrared spectrum of the complex [3a]

4. CONCLUSIONS

In this study, theoretical electronic and vibrational spectroscopic analyses of antimony (III) complexes were performed with B3LYP method GEN (C, H, N, Cl: 6-31G(d,p) and Sb: LanL2DZ) basis set. Six compounds' partial density of state diagram and the calculated PDOS contribution percentage have been investigated. The HOMO and LUMO orbitals are localized on mostly N-Sb-X (X: Cl, Br). As seen in the molecular electrostatic potential surface map, the negative charge is in the region on the N-Sb-Cl atoms. The calculation of first-order hyperpolarizability reveals that the [3b] complex has the lowest molecular dipole moment as μ = 0.25 Debye, β_{tot} ($\times 10^{-30}$) = 241.85 a.u. and it has a relatively higher average polarizability $\Delta\alpha$ (a.u.) value than the others. The RMS and mean average deviation of fundamental vibrations were found to be the average percentage error RMS was found to be 11.09, 12.64, and 14.26 for the [1a-3a] complexes, respectively. With the use of normal coordinate analysis, which was done by the scaled quantum mechanical force field methodology, the full interpretation of the vibrational spectra was carried out. According to RMS values, there is a fair agreement between experimental and predicted wavenumbers and assignments.

ACKNOWLEDGEMENTS

This study was supported by the Research Foundation of Hatay Mustafa Kemal University Project No: 16860. I would like to thanks the Gazi University for providing Gaussian 09W Software. The numerical calculations reported in this paper were performed at TUBITAK ULAKBIM, High Performance and Grid Computing Center (TRUBA Resources).

CONFLICT OF INTEREST

No conflict of interest was declared by the authors.

AUTHORSHIP CONTRIBUTIONS

Berna Çatıkkaş: Writing – review & editing, Supervision, Methodology, Investigation, Conceptualization, Methodology, Calculation. **Özge Şahinler:** Visualition, Editing.

REFERENCES

[1] Beyersmann D, Hartwig A. Carcinogenic metal compounds: recent insight into molecular and cellular mechanisms 2008; 82: 493–512.

[2] Krebs RE. The history and use of our earth's chemical elements: a reference guide. Greenwood Publishing Group 2006.

[3] Ulrich N. Antimony 2003; 81: 126.

[4] Estes JW. The medical skills of ancient Egypt. Science History Publications/USA 1993.

[5] Duffin J, René P. "Anti–moine; Anti–biotique": The Public Fortunes of the Secret Properties of Antimony Potassium Tartrate (Tartar Emetic) 1991; 46: 440–56.

[6] Herwaldt BL. Vol. 354 1999: 1191–99.

[7] Gielen M, Tiekink ERT. Metallotherapeutic drugs and metal-based diagnostic agents: the use of metals in medicine. John Wiley & Sons 2005.

[8] Mjos KD, Orvig C. Metallodrugs in Medicinal Inorganic Chemistry 2014; 114: 4540–63.

[9] Burford N, Carpenter Y, Conrad E, Saunders CDL. The Chemistry of Arsenic, Antimony and Bismuth. In: Hongzhe Sun, Ed. Biol. Chem. Arsenic, Antimony Bismuth.; John Wiley & Sons Ltd. 2011; pp. 1–18.

[10] Murray HW, Berman JD, Davies CR, Saravia NG. Advances in leishmaniasis 2005; 366: 1561–77.

[11] Newlove T, Guimarães LH, Morgan DJ, Alcântara L, Glesby MJ, Carvalho EM, et al. Antihelminthic therapy and antimony in cutaneous leishmaniasis: A randomized, double-blind, placebo-controlled trial in patients co-infected with helminths and leishmania braziliensis 2011; 84: 551–55.

[12] Baiocco P, Colotti G, Franceschini S, Ilari A. Molecular basis of antimony treatment in Leishmaniasis 2009; 52: 2603–12.

[13] Magill AJ, Strickland GT, Maguire JH, Ryan ET, Solomon T. Hunter's tropical medicine and emerging infectious disease. Elsevier Health Sciences 2012.

[14] Dostál L, Jambor R, Růžička A, Jirásko R, Černošková E, Beneš L, et al. [2 + 2] Cycloaddition of Carbon Disulfide to NCN-Chelated † Organoantimony(III) and Organobismuth(III) Sulfides: Evidence for Terminal Sb−S and Bi−S Bonds in Solution ‡ 2010; 29: 4486–90.

[15] Matsukawa S, Yamamichi H, Yamamoto Y, Ando K. Pentacoordinate Organoantimony Compounds That Isomerize by Turnstile Rotation 2009; 131: 3418–19.

[16] Moiseev DV, Morugova VA, Gushchin AV., Shavirin AS, Kursky YA, Dodonov VA. Tetraphenylantimony carboxylates in the cascade Pd-catalyzed C-phenylation reaction of methyl acrylate in the presence of peroxide 2004; 689: 731–37.

[17] Abboud KA, Palenik RC, Palenik GJ, Wood RM. Syntheses and structures of four antimony complexes with planar tridentate pyridine ligands 2007; 360: 3642–46.

[18] Prokudina Y V, Davydova EI, Virovets A, Stöger B, Peresypkina E, Pomogaeva A V, et al. Structures and Chemical Bonding in Antimony(III) Bromide Complexes with Pyridine 2020; 26: 16338–48.

[19] Davydova EI, Virovets A, Peresypkina E, Pomogaeva A V, Timoshkin AY. Crystal structures of antimony(III) chloride complexes with pyridine 2019; 158: 97–101.

[20] Tunç T, Koç Y, Açik L, Karacan MS, Karacan N. DNA cleavage, antimicrobial studies and a DFT-based QSAR study of new antimony(III) complexes as glutathione reductase inhibitor 2015; 136: 1418–27.

[21] Tunç T, Karacan MS, Ertabaklar H, Sarı M, Karacan N, Büyükgüngör O. Antimony(III) complexes with 2-amino-4,6-dimethoxypyrimidines: Synthesis, characterization and biological evaluation. 2015; 153: 206–14.

[22] Karacan MS, Rodionova MV., Tunç T, Venedik KB, Mamaş S, Shitov A V., et al. Characterization of nineteen antimony(III) complexes as potent inhibitors of photosystem II, carbonic anhydrase, and glutathione reductase 2016; 130: 167–82.

[23] Frisch MJ et al. Gaussian 09, Revision A.02 2009.

[24] O'boyle NM, Tenderholt AL, Langner KM. cclib: A library for package-independent computational chemistry algorithms 2008; 29: 839–45.

[25] Politzer P, Laurence PR, Jayasuriya K. Molecular electrostatic potentials: An effective tool for the elucidation of biochemical phenomena 1985; VOL. 61: 191–202.

[26] Politzer P, Murray JS. The fundamental nature and role of the electrostatic potential in atoms and molecules 2002; 108: 134–42.

[27] Hofacker GL. Peter Politzer und Donald G. Truhlar: Chemical Applications of Atomic and Molecular Electrostatic Potentials, Plenum Press, New York und London 1981. 472 Seiten, Preis: $ 55.- 1982; 86: 872–73.

[28] Kurtz HA, Stewart JJP, Dieter KM. Calculation of the nonlinear optical properties of molecules 1990; 11: 82–87.

[29] Fogarasi G, Zhou X, Taylor PW, Pulay P. The calculation of ab initio molecular geometries: efficient optimization by natural internal coordinates and empirical correction by offset forces 1992; 114: 8191–8201.

[30] Pulay P, Fogarasi G, Pongor G, Boggs JE, Vargha A. Combination of theoretical ab initio and experimental information to obtain reliable harmonic force constants. Scaled quantum mechanical (QM) force fields for glyoxal, acrolein, butadiene, formaldehyde, and ethylene 1983; 105: 7037–47.

[31] Parallel Quantum Solutions, SQM 2013.

[32] Parr RG, Szentpály L v, Liu S. Electrophilicity index 1999; 121: 1922–24.

[33] Koopmans T. Über die Zuordnung von Wellenfunktionen und Eigenwerten zu den Einzelnen Elektronen Eines Atoms 1934; 1: 104–13.

[34] Tunç T, Ertabaklar H, Karacan N. In vitro anti-leishmanial activities and structure-activity relationship analysis of new antimony(III) complexes 2020; 59: 1609–17.

[35] Andraud C, Brotin T, Garcia C, Pelle F, Goldner P, Bigot B, et al. Theoretical and experimental investigations of the nonlinear optical properties of vanillin, polyenovanillin, and bisvanillin derivatives 1994; 116: 2094–2102.

[36] Geskin VM, Lambert C, Brédas J-L. Origin of high second-and third-order nonlinear optical response in ammonio/borato diphenylpolyene zwitterions: the remarkable role of polarized aromatic groups 2003; 125: 15651–58.

[37] Socrates G. Infrared and Raman characteristic group frequencies. 2004.

[38] Varsányi G. Vibrational spectra of benzene derivatives. Elsevier 2012.

[39] Zickgraf A, Bräu E, Dräger M. As(III)/Sb(III)/Bi(III)–halide distances and stretching vibrations. An application of the Varshni relationship upon hypervalent group 15 compounds 1998; 54: 85–90.